Visualizing a Nonlinear Response in a Schrödinger Wave

Pengbo Jia,[1,§] Zhili Li,[1,§] Yi Hu,[1,*] Zhigang Chen,[1,2,†] and Jingjun Xu[1,‡]
[1]The MOE Key Laboratory of Weak-Light Nonlinear Photonics, TEDA Applied Physics Institute and School of Physics, Nankai University, Tianjin 300457, China
[2]Department of Physics and Astronomy, San Francisco State University, San Francisco, California 94132, USA

(Received 21 July 2019; published 4 December 2019)

We demonstrate for the first time that the nonlinear response of a medium can be mapped directly onto a dynamical wave profile as governed by a generalized nonlinear Schrödinger equation. As analyzed in an accelerating coordinate, the intrinsic gravitylike potential helps "isolate" the effects related to a strong repulsive nonlinear interaction from the dispersion or diffraction in a steady state. Thus, under appropriate conditions, the associated nonlinear response curve can be read out directly in the profile of the nonlinear state. A simple scheme is proposed to approach adiabatically these modes through a shaped input wave profile. Our analysis is further verified experimentally by directly visualizing a Kerr (saturable) nonlinearity experienced by an optical pulse (beam) in a nonlinear fiber (photorefractive crystal), validating the versatility of this approach for different types of optical nonlinearities.

DOI: 10.1103/PhysRevLett.123.234101

Wave dynamics governed by the nonlinear Schrödinger equation appear in many branches of physics. The combination of dispersive and nonlinear effects in this model leads to a variety of intriguing phenomena. (In the spatial domain, diffraction plays a role analogous to that of dispersion. For brevity of description, we shall use only the term "dispersion" or "dispersive" hereafter.) More fruitful dynamics have been found in a generalized configuration of this equation by employing various forms of nonlinearities [1–9]. As a reason for sculpturing a wave, the associated nonlinear response is likely to leave in the wave profile a footprint and hence becomes measurable, which could help explore and understand unknown nonlinear mechanisms. Unfortunately, thus far to our knowledge no evidence has shown that a nonlinear response can be displayed directly in a wave profile. This is partially due to the fact that a nonlinear effect generally cannot be separated from the dispersive effect. The best known example is the stationary soliton (either with bright or dark type) where the nonlinearity and the dispersion act together in a perfectly balanced manner [10,11]. For nonstationary dynamics, most phenomena from the common nonlinear evolution of Gaussian waves to some novel energy flows, such as dispersive shock waves [12] and rouge waves [13], are still mediated by the production of both factors. Although weak dispersions are required in some dynamics like Riemann wave generations [14,15], the problem of separating nonlinear and dispersive effects remains unsolved.

In this Letter, we demonstrate for the first time that the nonlinear response of a medium can be directly visualized in a wave of a system governed by a generalized nonlinear Schrödinger equation (GNLSE). In an accelerating frame, surprisingly, a repulsive nonlinearity can be isolated from the dispersive effect, and thus the associated nonlinear response can be read out by examining the nonlinear modes of this equation. The visualization becomes more precise for a solution experiencing a stronger nonlinearity. Via an adiabatic evolution, a properly shaped input can approach these nonlinear modes, and consequently can show the nonlinear response in its profile. The proposed method is further assessed in experiments with an optical fiber (exhibiting a Kerr-type nonlinearity) and a photorefractive crystal (exhibiting a saturable nonlinearity), validating the universality of the method.

We start our analysis with a GNLSE:

$$\frac{\partial\psi}{\partial\zeta} = \frac{i}{2}\frac{\partial^2\psi}{\partial\xi^2} - if(I)\psi, \tag{1}$$

where ψ is a wave packet that evolves along ζ axis and disperses along ξ axis, $f(I)$ is a real-valued algebraic function representing different types of the nonlinearity, and $I = |\psi|^2$ is the wave intensity. The sign of $f(I)$ (>0 or <0) is independent of the dispersion. As we will demonstrate in the following, it is possible to separate the nonlinear effect from the dispersive effect [associated with the second derivative term in Eq. (1)] in an accelerating coordinate. By using $s = \xi - h\zeta^2/2$ (h is a constant) and $\psi = u(s)\exp(ih^2\zeta^3/6 + ih\xi\zeta)$ (where u is a real-valued function), Eq. (1) can be rewritten in a steady state as:

$$\frac{d^2u}{ds^2} - 2hsu - 2f(I)u = 0. \tag{2}$$

Without loss of generality, we use a positive value of h for our following analysis. As seen from Eq. (2), a gravitylike

potential (experienced by a wave packet) is introduced in the accelerating frame [16]. In the absence of any nonlinearity, an Airy solution [16,17] is found in this potential, consisting of a main lobe and infinite sublobes toward the left [Fig. 1(a)]. Its semi-infinite configuration is attributed to the fact that only the right side of a wave experiences an infinite potential barrier. Since the nonlinearly induced potential cannot alter the infinite nature of the barrier considering the intensity limit of waves, a nonlinear solution for Eq. (2) is expected to have a similar structure as the Airy case [18–21]. Under an attractive nonlinearity, all the lobes tend to shrink compared to the linear case, thus experiencing a more intense dispersion. As a result, both the nonlinear and the dispersive effects contribute to the solutions. However, the scenario is changed under a repulsive nonlinearity. In this latter condition, although the sublobes having a configuration similar to an interference pattern are still afflicted with the dispersive effect, an expansion of the main lobe toward the right may reduce the influence of the dispersion. For a sufficiently wide main lobe expanded by a strong nonlinearity, the first term in Eq. (2) may be neglected, leading to a dominated nonlinear effect in the nonlinear state. Using this approximation, one has $[hs + f(I)]u = 0$ that can only be satisfied when $hs + f(I) = 0$. Without the influence of the dispersion term, the nonlinear effect plays a role to flatten the gradient potential to the level of zero. A typical solution (only the main lobe) in a strong nonlinear regime is shown in Fig. 1(b), where a repulsive Kerr nonlinearity is employed. The nonlinearly induced potential at the right side of the main lobe can almost counteract the gravitylike potential, which is in accord with our expectation. On the contrary, the left side, having a slope sign opposite to the right side, strengthens the steepness of the linear potential by the nonlinearity, violating the condition of $hs + f(I) = 0$, and further indicating the indispensability of the dispersion term. Therefore, the nonlinear effect can only be "isolated" for the right side of the main lobe.

When the dispersive effect is be safely neglected, as discussed above, one can obtain from Eq. (2):

$$s = -f(I)/h, \tag{3}$$

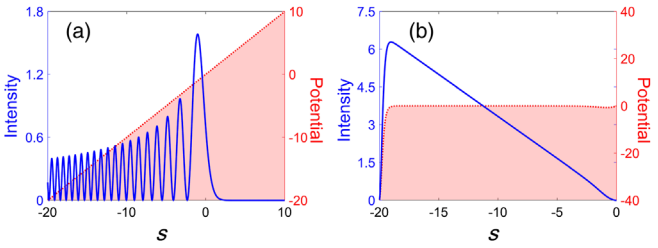

FIG. 1. (a) Typical linear and (b) nonlinear solutions (blue lines) of a GNLSE in an accelerating coordinate. The red shaded area in (a) corresponds to the gravitylike potential introduced in the accelerating frame, while that in (b) illustrates the effect of adding a nonlinearly induced potential to the potential in (a).

where one can infer that it is possible to project a nonlinear response to a transverse axis. In theory, let us assume three different types of nonlinearities for testing the visualization of the associated nonlinear responses. They take the form of $f(I) = n_2 I, n_2 I^{2/3}, n_2 I^2$ (n_2 is a constant), corresponding to the Kerr type, the type modeling the wave dynamics in zero-temperature Fermi gases [22,23], and a quintic nonlinearity associated with three-body interactions in Bose-Einstein condensates [24], respectively. In order to meet the approximation condition for deriving Eq. (3), solutions of a sufficiently high peak intensity (I_p) are concerned. The right sides of their main lobes are typically presented in Fig. 2(a) in a normalized form, where $n_2 = -3$ is adopted. Using Eq. (3), these intensity profiles are fitted well in almost the whole range [for the fitting here and in the following, we change the form of Eq. (3) into $(s-A)/B = f[(I-C)/D]$, where A, B, C, and D are fitting parameters]. Slight mismatches only appear at the two ends where dispersive effects still take place. By means of a higher peak intensity (indeed corresponding to a wider main lobe) for the nonlinear mode, the mismatched areas tend to become relatively smaller. To characterize the fitting, the following parameter is defined: $Q = 1 - \sqrt{\sum (F-I)^2 / \sum F^2}$, where F describes the fitting values. Lager Q indicates a higher similarity between the fitting and the target curves and $Q = 1$ reflects an exact overlapping. The inset of Fig. 2(a) presents the values of Q for a variety of nonlinear modes associated with the three types of nonlinearities. As expected, Q is larger for the case of a higher peak intensity, indicating that the dispersion has a less influence. In a stronger accelerating frame (i.e., larger h), a steeper gravitylike potential is introduced, so one should employ a wider (accordingly more intense) main lobe to relatively reduce the mismatched area for a better visualization. For instance, a higher peak intensity is required to realize the same degree of fitting (say, $Q = 0.985$) in a coordinate having a larger acceleration [Fig. 2(b)]. In any case, Q becomes saturable at the level of one if the peak intensity

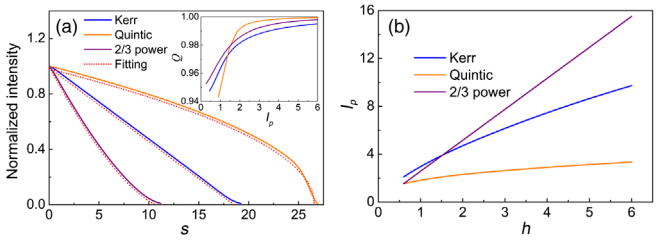

FIG. 2. (a) Nonlinear modes (only the right sides of the main lobes) under three different types of nonlinearities and the corresponding fitting curves (shifted artificially downward for a better comparison) calculated by employing Eq. (3). The inset presents the degree of fitting for different peak intensities of the nonlinear modes. (b) Peak intensities needed to reach the same degree of fitting (i.e., $Q = 0.985$) for the nonlinear modes in (a) in various accelerations of the coordinates.

approaches infinity. Hence, one can employ the nonlinear modes to visualize a nonlinear response as long as their peak intensities are kept high enough. Although our method can only work for a repulsive nonlinearity, we should note that it is possible to visualize a nonlinear term in a physical system that originally leads to an attractive nonlinearity. This can be achieved by reversing the sign of the dispersion or diffraction to satisfy the condition of a repulsive nonlinearity. In the following experiment, nonlinearities of both types will be considered and experimentally tested.

Inspired by the fact that a Gaussian wave packet can evolve into a soliton, it is possible to reach the previously solved nonlinear states through wave dynamics governed by Eq. (1). Along this line, the Airy function [i.e., the solution of Eq. (2) in the linear limit] can be used as the input [18,19]. To guarantee an adiabatic change (i.e., to reach a weak nonlinearity for early evolution), the Airy function is properly truncated and is preset to be far away from the input. For this purpose, one can multiply a Gaussian-like amplitude in the spectral domain (described by ω) by a phase modulation formulated as

$$\rho = \exp(ia\omega^3 + ib\omega^2), \tag{4}$$

where a and b are constants, the cubic term [17] is associated with the Airy function, and the quadratic one manages to deliver the Airy field toward the output in the linear case.

We now test our proposed method in experiment. In the first experiment, the Kerr-type nonlinearity is examined via pulse propagation through a nonlinear optical fiber [see the schematic setup in Fig. 3(a)]. The input pulse is obtained by initially shaping [via a pulse shaper (Finisar, 1000A)] and then amplifying [via an erbium-doped fiber amplifier (EDFA)] a broadband femtosecond pulse. According to our previous analysis, its spectrum is prepared by imposing a phase modulation expressed in Eq. (4), via the same pulse shaper. The nonlinear wave dynamics is performed in a dispersion shifted fiber (DSF) at hand (~3.9 km long) and the temporal output is characterized by means of a frequency-resolved optical gating (FROG) system (MesaPhotonics, MP-002). The pulse, centered at 1534 nm with a ~4 nm bandwidth, is located at the normal dispersion region of this fiber with a zero dispersion wavelength around 1547.7 nm, thus experiencing a repulsive nonlinear effect [14], although the Kerr nonlinearity in fibers typically has a positive sign. Before the nonlinear examination, an Airy pulse is preset to appear at the output of the DSF in the linear case by adopting $a = 0.2$ ps^3 and $b = 2.47$ ps^2 in the spectral phase modulation. Then larger values of powers from the EDFA are used to study the nonlinear case, while the other conditions are kept unchanged. Although the output pulse experiences a broadening as the power level is higher [Figs. 3(b)–3(d)], its trailing edge always exhibits a linear shape, fitted well by using Eq. (3) with a Kerr nonlinearity. Furthermore, the pulse

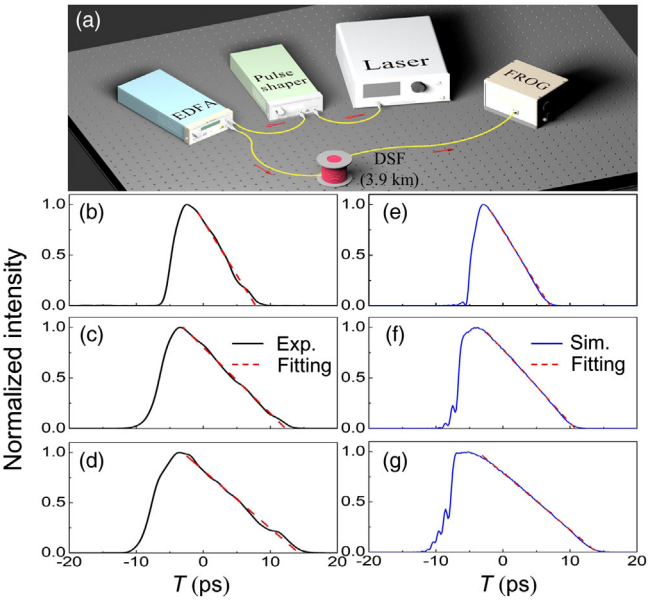

FIG. 3. (a) Schematic experimental setup for visualizing a Kerr nonlinearity. (b)–(g) Experimental results (left) and the corresponding numerical simulations (right) recording the nonlinear output in a DSF at different input power levels (2, 4, and 6 mW from top to bottom). The dashed straight lines (red) are from calculations by using Eq. (3) to fit the trailing edge of the pulse.

propagation is performed numerically using the following equation:

$$\frac{\partial\varphi}{\partial z} = -i\frac{\beta_2}{2}\frac{\partial^2\varphi}{\partial T^2} + \frac{\beta_3}{6}\frac{\partial^3\varphi}{\partial T^3} + i\gamma|\varphi|^2\varphi, \tag{5}$$

where φ is the field envelope of the pulse, z (or T) is the propagation distance (or the time delay), β_2 (>0) and β_3 are the coefficients of the second and the third order dispersion, and γ is the nonlinear coefficient. In the absence of the third order dispersion, Eq. (5) can be reshaped into Eq. (1) by using the relations $\psi/\varphi^* = \sqrt{\gamma T_0^2/\beta_2}$, $\xi/T = 1/T_0$, $\zeta/z = \beta_2/T_0^2$, and $f(I) = |\psi|^2$, where T_0 is a constant time length and the asterisk stands for the complex conjugation. In simulations, the experimental parameters, i.e., $\beta_2 = 6 \times 10^{-4}$ ps^2 m^{-1}, $\beta_3 = 1.2 \times 10^{-4}$ ps^3 m^{-1}, and $\gamma = 0.8 \times 10^{-3}$ W^{-1} m^{-1}, are employed. The numerical outputs [Figs. 3(e)–3(g)] have a good agreement with the experimental observations. Although the third order dispersion has been considered, it almost has no influence on our approach considering that the nonlinear length is much shorter than the third order dispersion length.

In the second experiment, we test our approach in the spatial domain (now diffraction appears instead of dispersion) for a saturable nonlinearity offered by a photorefractive crystal (SBN: 61) whose dimension is $5(x) \times 5(y) \times 10(z)$ mm^3 using the setup shown in Fig. 4(a). The nonlinearly induced refractive index change Δn is formulated as $-0.5n_0^3\gamma_{33}E_e/(1+I)$ [4,25], where

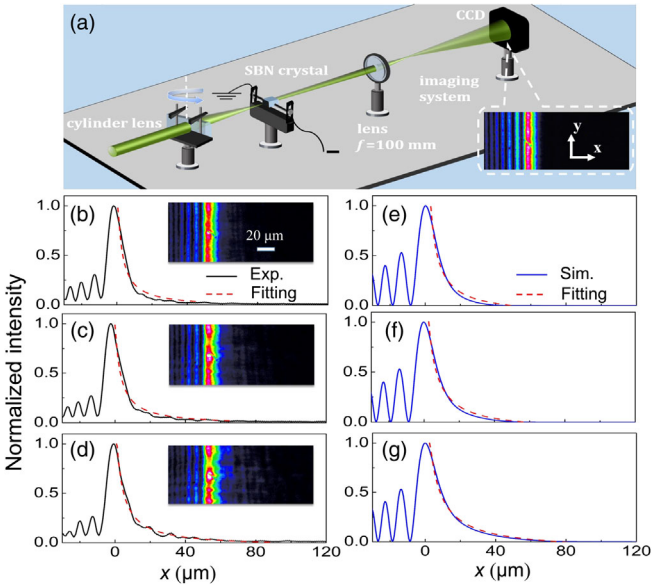

FIG. 4. (a) Schematic experimental setup for visualizing a saturable nonlinearity. (b)–(g) Experimental results (left) and the corresponding numerical simulations (right) recording the nonlinear output in a photorefractive crystal biased with different electric fields (−120, −140, and −180 kV/m from top to bottom). The dashed curved lines (red) in (b)–(g) are calculated by using Eq. (3) to fit the right edge of the main lobe. The intensity profiles in (b)–(d) are obtained by integrating vertically the output patterns in the corresponding insets. Note that the scale bar in (b) shows the dimension at the back face of the crystal.

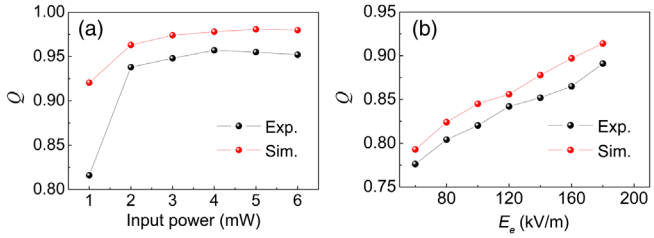

FIG. 5. Panels (a) and (b) show the similarity between fitting and target curves for the cases of (a) Kerr and (b) photorefractive nonlinearities obtained from both experiments and simulations.

$n_0 = 2.3$ is the unperturbed refractive index, $\gamma_{33} = 280$ pm/V is the electro-optic coefficient for the extraordinarily polarized beams, and E_e is the bias field. Applying a negative bias, nonlinearly-induced index changes are smaller for a higher light intensity, which is opposite to the case for the previously used Kerr nonlinearity. Thus the two types of nonlinearities require diffractions of opposite signs to reach a repulsive nonlinearity. The saturable nonlinear response is probed by an e-polarized Airy beam (at 532 nm) (generated by passing a Gaussian beam through a tilting cylindrical lens with a 50 mm focal length [26]). For the purpose of adiabatic evolution along the z direction, we adjust the position of the nonlinear medium to realize a quite weak nonlinearity for the probe near the input, rather than by employing a quadratic phase mentioned before to alter the beam propagation. In detail, the output facet of the crystal in the $x-y$ plane is positioned at the location where the Airy beam has the largest peak intensity in the linear case (i.e., without a bias field). The linear output, presented in the inset of Fig. 4(a), almost keeps invariant vertically while horizontally it can be described by a truncated Airy function. Considering the saturable effect of the photorefractive effect, the bias voltage (applied along the x direction) is employed to strengthen the nonlinearity for satisfying the condition of Eq. (3) while keeping the input power (6.3 mW) unchanged. As the voltage is turned up, the main lobe of the output exhibits a different scenario of broadening compared to the Kerr case. Its intense part (say, above 25% of peak intensity) is slightly wider yet its decay becomes slower toward the right under the action of a stronger nonlinearity [Figs. 4(b)–4(d)]. Slight oscillations in the right side of the beam profile are noticed. This may be caused by the modulation instability that can hardly keep the beam invariant vertically, as inferred from the insets of Figs. 4(b)–4(d). By using Eq. (3) together with the photorefractive nonlinearity to fit the right side of the main lobe, one can see that the fitting tends to be better for a higher voltage. The beam dynamics that is assumed to be invariant along the y direction is further simulated by using the following nonlinear Schrödinger equation:

$$\frac{\partial U}{\partial z} = \frac{i}{2k_0 n_0}\frac{\partial^2 U}{\partial x^2} + ik_0 \Delta n U, \tag{6}$$

where U is the optical field and k_0 is the vacuum wave vector. Equation (6) can be transformed into Eq. (1) by using the relations $U = \psi$, $\xi/x = 1/x_0$, $\zeta/z = 1/(k_0 n_0 x_0^2)$, and $f(I) = -k_0^2 x_0^2 n_0 \Delta n$, where x_0 is a constant spatial length. Again, the numerical results [Figs. 4(e)–4(g)] have almost a perfect agreement with the experimental observations.

Furthermore, the similarities characterized by Q for the results in Figs. 3 and 4 are summarized in Fig. 5. For the Kerr case, the value of Q is positively proportional to the strength of the nonlinearity until the input power is turned up to 4 mW where a saturation starts [Fig. 5(a)]. Such a result agrees with our previous analysis. For the photorefractive case, Q keeps going up with the bias field yet does not reach a saturable level in the range of applied voltages [Fig. 5(b)]. Additional simulations show that the saturation is possible for further increasing the voltage, but in experiment, we could not accordingly perform this test due to possible depolarization of our crystal.

In conclusion, we have demonstrated that the nonlinear response of a medium can be directly displayed in the profile of a Schrödinger wave. By analyzing the nonlinear modes of the GNLSE in an accelerating coordinate, we found that a repulsive nonlinear effect can be isolated from the dispersive one, thus mapping the associated response curve to the modes. Such a visualization can keep a high

fidelity under the action of a strong nonlinearity. To read out the nonlinear response, a properly shaped input is employed to approach these modes adiabatically. The theoretical and numerical findings are further verified experimentally for visualizing two distinct nonlinearities with different types (Kerr and saturable). Our proposed method, merely relying on a shaped input, has the potential to be extended into other physical systems for the characterization of nonlinear responses.

We acknowledge financial support from the National Key R&D Program of China (2017YFA0303800), the National Natural Science Foundation of China (NSFC) (61575098, 91750204), and the 111 Project in China (B07013).

*yihu@nankai.edu.cn
†zgchen@nankai.edu.cn
‡jjxu@nankai.edu.cn
§P. J. and Z. L. contributed equally to this work.

[1] D. Mihalache, M. Bertolotti, and C. Sibilia, Prog. Opt. **27** (1989).
[2] S. Giorgini, L. P. Pitaevskii, and S. Stringari, Rev. Mod. Phys. **80**, 1215 (2008).
[3] M. Segev, B. Crosignani, A. Yariv, and B. Fischer, Phys. Rev. Lett. **68**, 923 (1992).
[4] D. N. Christodoulides and M. I. Carvalho, J. Opt. Soc. Am. B **12**, 1628 (1995).
[5] B. L. Lawrence, M. Cha, J. U. Kang, W. Toruellas, G. Stegeman, G. Baker, J. Meth, and S. Etemad, Electron. Lett. **30**, 447 (1994).
[6] S. D. Martino, M. Falanga, C. Godano, and G. Lauro, Europhys. Lett. **63**, 472 (2003).
[7] P. Kaw, G. Schmidt, and T. Wilcox, Phys. Fluids **16**, 1522 (1973).
[8] Y. S. Kivshar, Opt. Quantum Electron. **30**, 571 (1998).
[9] Y. V. Kartashov, G. E. Astrakharchik, B. A. Malomed, and L. Torner, Nat. Rev. Phys. **1**, 185 (2019).
[10] V. E. Zakharov and A. B. Shabat, Sov. Phys. JETP **34**, 62 (1972).
[11] Y. S. Kivshar and B. Luther-Davies, Phys. Rep. **298**, 81 (1998).
[12] A. V. Gurevich and A. L. Krylov, Zh. Eksp. Teor. Fiz. **92**, 1684 (1987).
[13] N. Akhmediev, A. Ankiewicz, and J. M. Soto-Crespo, Phys. Rev. E **80**, 026601 (2009).
[14] B. Wetzel, D. Bongiovanni, M. Kues, Y. Hu, Z. Chen, S. Trillo, J. M. Dudley, S. Wabnitz, and R. Morandotti, Phys. Rev. Lett. **117**, 073902 (2016).
[15] D. Bongiovanni, B. Wetzel, P. Yang, Y. Hu, Y. Qiu, J. Xu, S. Wabnitz, Z. Chen, and R. Morandotti, Opt. Lett. **44**, 3542 (2019).
[16] M. V. Berry and N. L. Balazs, Am. J. Phys. **47**, 264 (1979).
[17] G. A. Siviloglou, J. Broky, A. Dogariu, and D. N. Christodoulides, Phys. Rev. Lett. **99**, 213901 (2007).
[18] A. Lotti, D. Faccio, A. Couairon, D. G. Papazoglou, P. Panagiotopoulos, D. Abdollahpour, and S. Tzortzakis, Phys. Rev. A **84**, 021807(R) (2011).
[19] C. Ruiz-Jimenez, K. Z. Nobrega, and M. A. Porras, Opt. Express **23**, 8918 (2015).
[20] R.-P. Chen, C.-F. Yin, X.-X. Chu, and H. Wang, Phys. Rev. A **82**, 043832 (2010).
[21] I. Dolev, I. Kaminer, A. Shapira, M. Segev, and A. Arie, Phys. Rev. Lett. **108**, 113903 (2012).
[22] J. A. Joseph, J. E. Thomas, M. Kulkarni, and A. G. Abanov, Phys. Rev. Lett. **106**, 150401 (2011).
[23] S. K. Adhikari, Phys. Rev. A **77**, 045602 (2008).
[24] B. Damski, Phys. Rev. A **69**, 043610 (2004).
[25] Y. Hu, S. Huang, P. Zhang, C. Lou, J. Xu, and Z. Chen, Opt. Lett. **35**, 3952 (2010).
[26] D. G. Papazoglou, S. Suntsov, D. Abdollahpour, and S. Tzortzakis, Phys. Rev. A **81**, 061807(R) (2010).